SN Computer Science (2022) 3: 332
https://doi.org/10.1007/s42979-022-01217-7

ORIGINAL RESEARCH

Tunnel Vision Hypothesis: Cognitive Factor Affecting Crowd Evacuation Decisions

Akira Tsurushima[1]

Received: 11 September 2021 / Accepted: 18 May 2022 / Published online: 13 June 2022

Abstract

Numerous studies have found the cognitive factors regarding crowd evacuation behaviors to be significant. However, because objective data are lacking, the exact effects of these factors have yet to be clarified. A video clip captured during the Great East Japan Earthquake involving 48 people in a meeting room gave researchers a unique opportunity to access data that allowed a numerical analysis of evacuation behaviors. Using the video clip, researchers discovered a unique evacuation behavior; the decision to either flee or drop was determined by a person's distance from the exit. Simulations using the evacuation decision model were conducted. The evacuation decision model is a model of herd behaviors that occur during evacuations, and the aforementioned unique evacuation behavior was successfully reproduced in the model. However, the simulation settings seemed to be oversimplified (e.g., number of agents, initial arrangement of the agents, disregarded physical constraints, etc.). This study aimed to reproduce the diagonal spatial pattern of evacuation decisions that emerged using new simulation settings that are more representative of the situation depicted in the video. The diagonal spatial pattern can only be reproduced within the limited ranges of two parameters that define the shape of the visual field of an agent—an autonomous entity in the simulation. The analysis of simulation results revealed that during evacuations, the visual field of an agent was narrowed to 20° with a relatively long range and led to a hypothesis that people undergoing evacuations were subject to tunnel vision, a cognitive effect in which excessive cognitive demands, fear, or mental stress narrows visual fields of people.

Keywords Herd behavior · Crowd dynamics · Multi-agent simulation · Evacuation decision-making

Introduction

Extensive research has been conducted within the fields of crowd dynamics, pedestrian movement, and evacuation behaviors. The amount of literature on empirical studies in these fields has been growing rapidly [18, 19]. The mental mechanisms and cognitive processes of people during evacuations have yet to be clarified due to the absence of objective numerical data, even though numerous researchers consider the mechanisms and processes to be significant [20, 46]. Thus, the studies in these fields are mainly conducted through interviews of survivors [13, 35], laboratory experiments with humans [16, 20, 45], or using animal subjects [25, 44]. However, each of these approaches has limitations regarding objectivity. This is because reproducing the mental stress and complexities present during a real evacuation situation in a laboratory experiment is difficult. Moreover, when studying survivors of real evacuations, researchers can only conduct interviews. It is well known that post-occurrence interviews are subject to survivorship bias. However, recently, some new evidence has come to light that is both capable of being quantified and analyzed. This evidence is a video of evacuation behavior exhibited by humans during a live evacuation. It is becoming more common that people have access to these moments, mostly owing to the increase of surveillance cameras and smartphones. Novel approaches to evacuation studies utilize these images and videos to enhance our understanding [12, 17, 59].

When analyzing the video clip captured during the Great East Japan Earthquake, a unique evacuation behavior in people regarding the decision to either flee the room or drop

This article is part of the topical collection "Agents and Artificial Intelligence" guest edited by Jaap van den Herik, Ana Paula Rocha and Luc Steels.

✉ Akira Tsurushima
a-tsurushima@secom.co.jp

[1] Intelligent Systems Laboratory, Secom Co., Ltd, Tokyo, Japan

cover and hold on was discovered. The analysis revealed that a person's actions depended upon their distance from the exit [50]. Numerous studies have been conducted pertaining to herd behavior during evacuations [1, 22, 32, 41] and the evacuation decision model, which represents herding in crowd evacuations, was proposed [47]. The unique evacuation behavior mentioned above was successfully reproduced using simulations employing the evacuation decision model, and it was concluded that herd behaviors are sufficient to reproduce the unique evacuation behavior [51]. However, these results might be limited in their relevancy, owing to oversimplified settings and assumptions. Some of these assumptions include the number of agents, the initial arrangement of these agents, and disregarded physical constraints.

The aim of this study is twofold. The first aim was to validate the previous result [51]. To do so, the simulations with settings that were more representative of the situations in the video were conducted to reproduce the diagonal spatial pattern of evacuees' decisions of fleeing and dropping. Second, to identify some of the unknown but critical cognitive factors affecting evacuees during crowd evacuations, the simulation results were analyzed and attempted to clarify the essential factors, so that the diagonal spatial pattern could be reproduced. A hypothesis that evacuees are subject to a cognitive factor called *the tunnel vision effect*, which has hardly been mentioned in the evacuation studies, was obtained in this analysis.

The model and our new findings could be employed to predict evacuation behaviors of people in indoor situations and also used to develop efficient evacuation protocol designs. Furthermore, these results might not be limited to earthquake evacuation, but are expendable to general evacuation situations that involve evacuation decisions.

This paper is the extended version of our previous paper [52]. The main differences between the two are as follows. First, the analysis of conditions between two simulation settings was added, as the previous settings were not as realistic as our new and improved settings. The simulation's settings are essential to reproducing the diagonal spatial pattern. The second is the analysis of the influence among agents critical in evacuation decisions during herd behaviors. The former is given in the *Comparative Analysis Between Simulation A and B* section, and the latter is given in the *Influence Analysis* section.

Related Work

Mackworth introduced the concept of the useful field of view, later called the functional field of view by many researchers. The functional field of view refers to *the area around the fixation point from which the information is briefly stored and read out during a visual task* [34]. To prevent mental overload, humans' functional field of view is narrowed by stressful, emotional, and unsafe events. The attention of people is focused on foveal, and objects in peripherals are often disregarded. Mackworth called this phenomenon *tunnel vision*. Two models were proposed to explain the tunnel vision effect: the general interference model and the tunnel vision model. The general interference model accounts for the tunnel vision effect as, independent of eccentricity, the sensitivity in peripherals being uniformly impaired, which increases as cognitive tasks become more complex [23]. In contrast, in the tunnel vision model, the loss of sensitivity in peripherals increases disproportionally with eccentricity [7].

Several studies have reported that emotional arousal strengthens the memory for central information but undermines the memory for peripheral information; Loftus et al. showed that memory related to weapons and details of the hand holding is improved at the expense of the face memory and objects in peripheral vision [31]. Furthermore, Christiansen and Loftus pointed out that the concept of central information was unclear in these studies [8, 9]. Discriminating central information into episode centrality and spatial centrality, Burke et al. revealed that emotional arousal prevents only the memory of spatially peripheral information [6]. Moreover, unusualness and a lack of safety play a role in the impairment of the functional field of view [21].

Research regarding tunnel vision is conducted extensively in the automotive and aviation industries. Thus, Miura measured the functional field of view of drivers, while they were driving and revealed that the visual field narrowed as traffic congestion increased [36]. Recarte and Nunes investigated the effects of mental workload tasks on visual detection and discrimination during driving [42]. Loss of attention causes critical consequences in the aviation industry. The effect of tunnel vision on air traffic control has been investigated to design a cognitive countermeasure to mitigate failure to pay attention [43]. The pilot's attention on a head-up display of an aircraft was studied to mitigate the failure of detecting object-based visual attention [24]. Some researchers in these fields also measured the angle of a visual field during tunnel vision of 2.2° [57], 7° [10], or 10°, [40].

Studies on tunnel vision revealed that stressful, unsafe, and unusual situations narrow human visual fields. These results imply that tunnel vision may occur during evacuation, because evacuation situations lead to all these experiences. However, research on tunnel vision or the functional field of view during evacuations has yet to be conducted extensively. Human vision-related studies regarding evacuations have mainly been conducted under the following two contexts: the identification of visual evacuation signs [2, 11, 15, 29, 38] and evacuation behaviors under limited visibilities [27, 28, 39]. Several researchers conducted experiments

using eye-tracking devices to investigate the direction in which evacuees were looking during evacuations [2, 11, 29]. The visual fields of pedestrians in normal situations were investigated using virtual reality devices, and the result that the visual fields are narrowed and focused more on people in front of them as the density increased was obtained [3]. Although these works do not focus on the functional field of vision of evacuees, the devices may be useful to reveal the functional field of view and tunnel vision effects during evacuations.

Numerous simulation models in evacuation studies have considered the visual field of an agent. However, in most cases, the size and shape of the functional field of view of an agent was arbitrarily determined. Clearly, this implies that the effects of tunnel vision have yet to be considered. Some of these simulations employ the cellular automaton-based model [28, 58, 61] and the social force model [33, 60, 62]; these models determine the visual field of an agent by distance, implying that the angle of the agent's vision is 360°. Other assumptions regarding the visual field angles adopted by researchers include 60° [35] and 90° [37]. Filippidis et al. [14] introduced the concept of visibility catchment area (VCA), which is the physical visibility range of an evacuation sign. They also assumed that an agent could recognize the evacuation sign in the VCA based on the probability obtained by the relative angle between the location of the sign and the traveling vector of the agent. These probabilities were arbitrarily selected and remained unchanged during simulations.

Evacuation Behavior During the Great East Japan Earthquake

A video clip[1] of the 48 people in the hotel meeting room (Fig. 1), captured during the Great East Japan Earthquake was analyzed [50]. This video is a unique occurrence of objective data of evacuation behaviors that allowed numerical analysis, which was possible for the following reasons:

1. The positions of all 48 people during the start of the earthquake were clearly captured;
2. The evacuation behaviors of all 48 people were captured in a continuous scene, from the beginning to the end of the earthquake; and
3. It was relatively easy to follow the behavior of each individual during evacuation (except a few evacuees).

The behavior of each evacuee in the video clip was manually analyzed every second. The behavior of some evacuees (e.g., 6 ⋯ 8 or 12 ⋯ 15 in Fig. 1) were not possible to follow because of occlusions and the small camera frame.

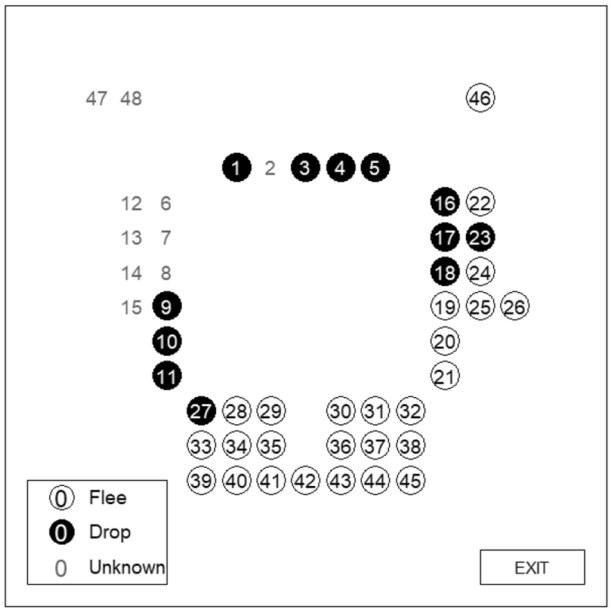

Fig. 1 The initial positions and evacuation decision of the 48 people in the hotel meeting room

Diagonal Spatial Pattern

Figure 1 depicts the initial positions of 48 people facing the center of a square meeting room at the beginning of the earthquake. The sole exit was at the bottom-right corner. Each person in the video chose one of two evacuation behaviors, either fleeing from the room or dropping and hiding under the tables. Figure 1 illustrates the evacuees' final evacuation decisions as taken by the people at their initial positions. A white circle depicts an evacuee who selected the fleeing behavior. The black circle depicts an evacuee who opted for the dropping behavior. The 48 people are represented by numbers; a gray number shows an evacuee whose choice to flee or drop is unknown. However, note that the behavior of evacuee 2 is unique. Evacuee 2 took neither fleeing nor dropping, but stood up and stayed near the wall behind during the shaking. Evacuee 2 is discluded in the analysis for simplicity and labeled unknown (Fig. 1).

In Fig. 1, the fact that those closest to the only exit overwhelmingly chose to flee, while those who were farther from the exit predominantly chose to drop was observed. Through this, the diagonal spatial pattern of the choices between fleeing and dropping emerged. Prior to this study and the presented simulation, the understanding that evacuees' evacuation behavior during an earthquake was determined by their distance from the exit did not exist. To our best knowledge, it was yet to be reported in the literature.

[1] https://www.fnn.jp/common/311/articles/201103110012.html.

There are two theories that are possibly accounting for this phenomenon:

1. The decisions between fleeing and dropping were determined by the distance from the exit; and
2. whereas each evacuee randomly selected fleeing and dropping, and herd behaviors among evacuees automatically allowed the diagonal spatial pattern to emerge.

The first theory is simple and easy to understand. However, it requires that high-level cognitive functions during a crisis, such as estimating the distance to the exit, thresholds to discriminate two decisions, and evacuation behavior selection rules based on the distance. In contrast, the second theory only requires herd behavior, which is a fundamental mechanism common to numerous social organisms, including birds, insects, fish, and animals. This study focused on herd behaviors during evacuation situations, and the second theory was adopted as our hypothesis when investigating human evacuation behaviors.

Evacuation Decision Model

The evacuation decision model [47] was developed to represent the herd behaviors of evacuees during evacuations. The evacuation decision model is a bio-inspired distributed algorithm based on the response threshold model [4, 5]. The response threshold model is a model of the division of labor in eusocial animals, often employed in biology. The evacuation decision model was employed to analyze evacuation behaviors of people in multiple exit environment and successfully reproduced the phenomenon called symmetry breaking in exit choice [48, 49]. The model is also used to explore an optimal arrangement of visual evacuation signs for an evacuation guidance signage system for efficient evacuations [53, 55], and to investigate the visual field of an agent in evacuations [54]. The analysis was conducted to investigate and reproduce the diagonal spatial pattern of selecting to either flee or drop using the evacuation decision model.

In the evacuation decision model, an agent a_i has a variable $X_i = \{1, 0\}$, and the agent's evacuation behavior depends on the value of X_i; a_i intentionally determines his/her evacuation behavior by himself/herself if $X_i = 1$; however, a_i unintentionally determines the behaviors by herd behavior if $X_i = 0$. The values of X_i toggle between 0 and 1 with the following transition probabilities:

$$P(X_i = 0 \to X_i = 1) = \frac{s_i^2}{s_i^2 + \theta_i^2} \tag{1}$$

$$P(X_i = 1 \to X_i = 0) = \epsilon, \tag{2}$$

where s_i is a local estimate of the stimulus from the environment for a_i, θ_i is the response threshold of a_i, and ϵ is a constant probability common to all the agents in a simulation. The local estimate of the stimulus of agent s_i at time $t + 1$ is calculated by

$$s_i(t+1) = \max\{s_i(t) + \delta - \alpha(1 - R)F, \ \ 0\}, \tag{3}$$

where δ is the increase of the stimulus per unit time, α is the scale factor of the stimulus, and R is the risk-perception function of objective risk r

$$R(r) = \frac{1}{1 + \mathrm{e}^{-g(r-\mu_i)}}, \tag{4}$$

where g is the activation gain of the sigmoid function and μ_i is the risk-perception factor of a_i, which represents the individual sensitivity to risk. The objective risk in the environment is

$$r(0) = 0, \tag{5}$$

$$r(t+1) = r(t) + \Delta r, \tag{6}$$

where Δr represents a risk increment at a unit time. F is the evacuation progress function of a_i, which estimates the total progress of the entire evacuation

$$F(n) = \begin{cases} 1 - n/\hat{N} & n < \hat{N} \\ 0 & \text{otherwise,} \end{cases} \tag{7}$$

where n is the number of agents within the visual field of a_i and $\hat{N}$ denotes the maximum possible number of agents in the visual field. The visual field of an agent is assumed to be a fan with radius d (units) and angle ω (degrees) from the direction of the agent's head. An agent performs one of two evacuation behaviors, depending on the value of X_i, as follows:

1. Randomly selects a fleeing or dropping behavior if $X = 1$ (random selection) or
2. Follows the most popular behaviors taken by the agents within the visual field if $X = 0$ (herd behavior).

No other rules (e.g., determining the behavior based on the distance from the exit) are incorporated into an agent's decision.

Simulation A

Simulations with simple settings using the evacuation decision model were conducted to reproduce the diagonal spatial pattern of fleeing and dropping behaviors; these simulation settings are referred to as Simulation A. In Simulation A, 500 agents were evenly distributed in a square

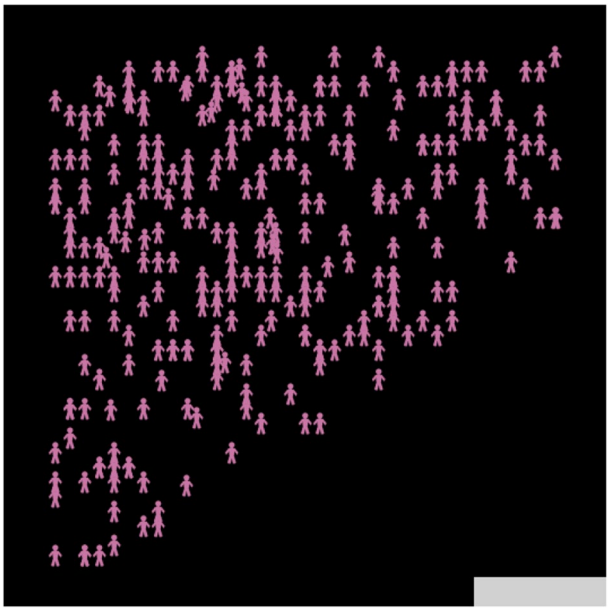

Fig. 2 Example of the diagonal spatial pattern. All fleeing agents went out through the exit and all dropping agents were in the room. A diagonal border between fleeing and dropping agents has emerged

space $S_A = \{(x, y) \in \mathbb{R}^2\}$, where $x, y \in [-20, 20]$, with only one exit at the lower right corner. The parameters employed in simulation A were $\alpha = 1.2$, $\delta = 0.5$, $\epsilon = 0.2$, $g = 1.0$, $\hat{N} = 10$, $d = 5$, and $\omega = 120$. These values are obtained through several experiments and are consistent with the values used in Ref. [50]. Figure 2 depicts an example result of Simulation A. All fleeing agents disappeared through the exit, while all dropping agents remained in an area far from the only exit, which resulted in the diagonal spatial pattern. From this, it was concluded that simple herd behaviors were sufficient to reproduce the diagonal spatial pattern [50, 51].

Critical Analysis

Simulation A demonstrated that the evacuation decision model could generally reproduce the diagonal spatial pattern. However, whether the evacuation decision model could be validated against a real evacuation situation, as depicted in the video, remains uncertain. This is because the initial conditions of Simulation A might not be considered the same as the conditions present in the video.

The environment of Simulation A, which was a square room with an exit at one corner, may be a good representation of the real situation in the video. However, the initial conditions of the agents in the environment are very different from those in the video. The number of agents in Simulation A totaled 500, whereas merely 48 evacuees were observed in the video. In Simulation A, the agents were randomly distributed across the room with high density. Meanwhile, in the real situation, the evacuees were arranged in a square shape with relatively sparse distribution across the room. Furthermore, agents faced random directions at the beginning of Simulation A. In the video of the real evacuation, people were facing the center of the room. Similarly, in the video, tables and chairs were laid out in a square shape, and all people were seated on these chairs when the earthquake began. Therefore, people's movements in the real situation were restricted by these objects. In contrast, the simulated agents were unrestricted physically and could directly access the exit in Simulation A.

In the evacuation decision model, the decision of an agent is affected by the decisions of the other agents within the agent's visual field. Therefore, the position of an agent in the room affects the decisions of the other agents and vice versa. Thus, which agents are within someone's visual field is crucial. The following factors are considered to affect the overall dynamics of the simulations with the evacuation decision model:

1. Constraints against the movement of an agent.
2. Direction in which the agent is facing.
3. Distribution of agents in the room.

For these reasons, the differences between Simulation A and those in the real situation in the video were too significant to ignore. Thus, extensive studies of these differences are desirable.

Method

In this study, simulations with new settings that could be considered as more representative of the real situation depicted in the video were conducted. As it was desired to reproduce the diagonal spatial pattern, these new settings were important to the research and subsequent analysis. Hereinafter, the simulation with the new settings is referred to as Simulation B. The evacuation decision model, which is used in Simulation A, is also incorporated in an agent in Simulation B. However, the initial settings of agents and the effects of physical constraints upon the agents are different.

Simulation B

To match the video, the number of agents in Simulation B is 48. In addition, these agents were arranged in a square in the space $S_B = \{(x, y) \in \mathbb{R}^2\}$, where $x, y \in [-7, 7]$, with one exit in the lower right corner (Fig. 3). As in the video, all

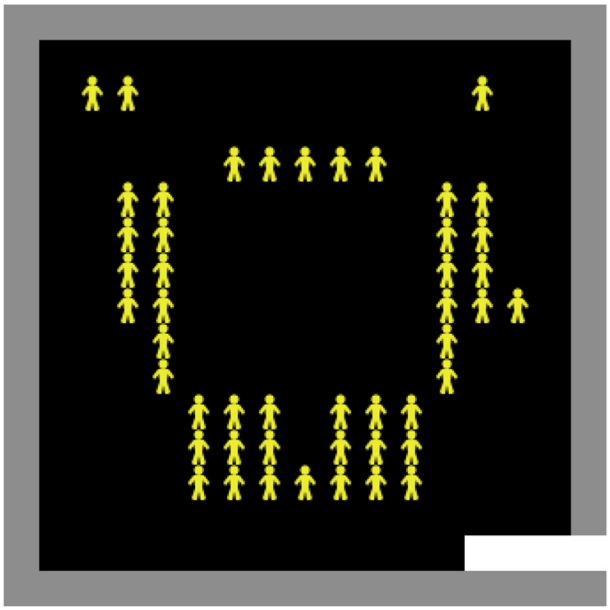

Fig. 3 Initial arrangement of 48 agents. [52]

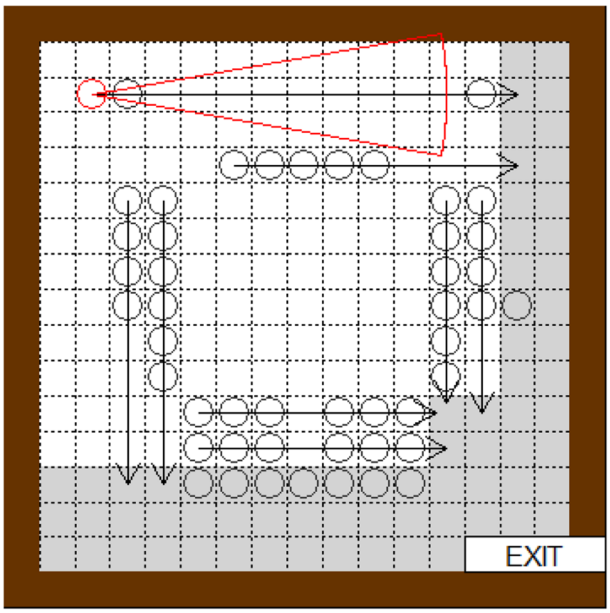

Fig. 4 Constraints on the movement of agents. Arrows depict the movement direction. The gray area indicates the spots where the movements of agents are unrestricted. The red fan shape shows the visual field of the red agent on the upper left corner [52]

agents faced the center of the room at the beginning of the simulation.

Figure 4 depicts constraints on the agent movement. A white circle signifies an agent at their initial position. An arrow on the grids shows the direction that an agent on the grid must follow. For example, the red agent in the upper left corner should move to the right, because the arrow on this grid points in the right direction. Gray grids signify the area in which the movement of an agent is unrestricted. Thus, when an agent reaches the gray grids, that agent can move directly toward the exit.

Table 1 Differences between Simulation A and Simulation B

	Simulation A	Simulation B
Number of agents	500	48
Initial position	Random	Square shaped
Density	Dense	Sparse
Facing direction	Random	Center of the room
Physical constraint	Disregarded	Considered

A significant difference between Simulations A and B is the implementation of physical constraints on the movements of the agents. In Simulation A, the movement of an agent is unrestricted. Therefore, an agent can move freely, even moving over other agents standing in the way of the exit. In contrast, the movement of an agent in Simulation B is constrained physically. Hence, the agent cannot walk through other agents and must stop if other agents stand in front of them. Although configurations are different, the evacuation decision model incorporated in Simulation B is identical to one employed in Simulation A.

Because the second theory accounting for the diagonal spatial pattern was adopted as our hypothesis, an agent with our model does not always behave as a human would behave. For example, agent 33 always follows agent 34 (Fig. 1) in our simulation, whereas a person at this position directly moves to the exit in the video. The reason why the movement of an agent is constrained rather than introducing physical objects in the environment and making an agent find its path to the exit is to avoid incorporating high-level cognitive functions in the model and to keep the model simple. For this reason, the same agent model can be used for both simulations.

Differences between Simulations A and B are summarized in Table 1. Here, conditions in Simulation A can be considered to be a more relaxed version of the constraints implemented in Simulation B. Thus, Simulation B was regarded as a specific sub-case of the more generalized Simulation A.

Simulation Model

In this section, the simulation algorithms employed in Simulation B are described. The algorithms are identical to those used in Ref. [50].

Algorithm 1 Herd behavior $(X = 0)$

$I^d \Leftarrow \{a_j \in V_i \mid \pi_j(t) = drop\}$
$I^f \Leftarrow \{a_j \in V_i \mid \pi_j(t) = flee\}$
$I^u \Leftarrow \{a_j \in V_i \mid \pi_j(t) = undecided\}$
if $|I^d| > |I^f|$ **and** $|I^d| > |I^u|$ **then**
  $\pi_i(t) \Leftarrow drop$
  $E_i^d \Leftarrow E_i^d \cup I^d$
else if $|I^f| > |I^d|$ **and** $|I^f| > |I^u|$ **then**
  $\pi_i(t) \Leftarrow flee$
  $E_i^f \Leftarrow E_i^f \cup I^f$
end if
if $\pi_i(t) = flee$ **then**
  move 1 unit following the constraints in Fig. 4.
end if

Algorithm 2 Random selection $(X = 1)$

if $\pi_i(t) = undecided$ **then**
  $\tau \sim U(0, 1)$
  if $\tau \leq 0.5$ **then**
    $\pi_i(t) \Leftarrow drop$
  else
    $\pi_i(t) \Leftarrow flee$
  end if
end if
if $\pi_i(t) = flee$ **then**
  move 1 unit following the constraints in Fig. 4.
end if

Algorithm 3 Simulation

for $t = 1$ to T **do**
  $r \Leftarrow min\{r + \Delta r,\ 100\}$
  for all $a_i \in A$ **do**
    Calculate s_i, R, and F (eq. 3, 4, and 7)
    $\tau \sim U(0, 1)$
    if $X_i = 1 \wedge \tau < P(X_i = 1 \rightarrow X_i = 0)$ **then**
      $X_i \Leftarrow 0$
    else if $X_i = 0 \wedge \tau < P(X_i = 0 \rightarrow X_i = 1)$ **then**
      $X_i \Leftarrow 1$
    end if
    if $X_i = 0$ **then**
      Execute Algorithm 1 {Herd Behavior}
    else if $X_i = 1$ **then**
      Execute Algorithm 2 {Random Selection}
    end if
    if a_i is on the exit **then**
      $A \Leftarrow A \setminus a_i$
    end if
  end for
end for

$A = \{a_1, a_2, \ldots, a_{48}\}$ is a set of 48 agents arranged on S_B, as shown in Fig. 3). Agent a_i has variable $\pi_i = \{\text{drop}, \text{flee}, \text{undecided}\}$, and holds the current decision. The visual field of a_i is defined as $V_i = \{a_j \in A \mid \nu(a_j, a_i)\}$, where $\nu : A^2 \rightarrow \{\text{true}, \text{false}\}$ and ν refer to a fan-like range of d units ω degrees toward the direction of motion of a_i. Agent a_i has two more variables, E_i^d and E_i^f, holding agents who are affected in their decision to drop or flee because of herd behavior.

An agent executes the action described in Algorithm 1 (Herd Behavior) if $X = 0$, and performs the action in Algorithm 2 (Random Selection) if $X = 1$. The values of $X = 1$ and 0 interchange with the probability given by the evacuation decision model. Assuming a simulation time $t = 1, \ldots, T$, the overall procedure is given in Algorithm 3

NetLogo 6.1.1 [56] was used to implement the algorithms described in this section.

Model Parameter

The model in Simulation B has eight parameters, ϵ, δ, α, d, ω, Δr, $\hat{N}$, and g. These parameters affect the simulation results; thus, the emergence of diagonal spatial pattern is dependent on these values. These parameter values must be adjusted to obtain the diagonal spatial pattern.

For this purpose, an objective function $O : S_B \rightarrow \mathbb{R}$, which evaluates the simulation results in terms of the occurrence of the diagonal spatial pattern, was developed. By considering the center of the room as the origin, function O must consider the following two conditions:

1. Maximize the total distance between the agents and the line $y = x$ if they are above the line; minimize the total distance between the agents and the line if they are below the line.
2. Equalize the total distance from the line $y = -x$ to the agents above and below the line.

The coordinates of agent remained as a_i be (x_i, y_i). Condition 1 can be expressed by maximizing

$$L^+ = \sum_{\{a_i | y_i \geq x_i\}} l_i^+ - \sum_{\{a_j | y_j < x_j\}} l_j^+, \tag{8}$$

where l_i^+ is the distance between a_i and $y = x$

$$l_i^+ = \sqrt{2\left(\frac{x_i - y_i}{2}\right)^2}. \tag{9}$$

Condition 2 can be expressed by minimizing

$$L^- = \left| \sum_{\{a_i | y_i \geq -x_i\}} l_i^- - \sum_{\{a_j | y_j < -x_j\}} l_j^- \right|, \tag{10}$$

where l_i^- is the distance between a_i and $y = -x$

$$l_i^- = \sqrt{\left(x + \frac{y - x}{2}\right)^2 + \left(y - \frac{y - x}{2}\right)^2}. \tag{11}$$

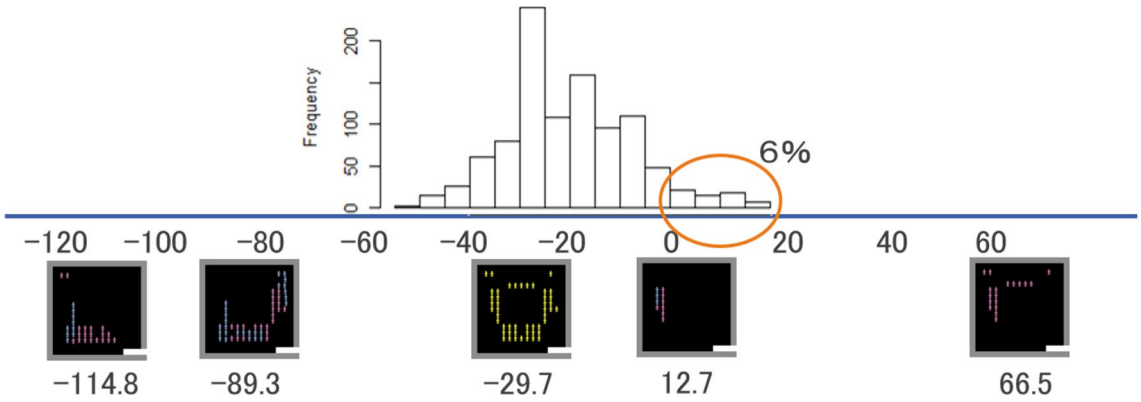

Fig. 5 Histogram of the values of $\bar{O}$ for 1000 simulations with random parameters and some spatial pattern examples with O

Thus, the diagonal spatial pattern can be obtained by

$$\text{maximize} \quad O = L^{+} - L^{-} \tag{12}$$

with respect to the domains of the parameters in the model.[2] Examples of a spatial pattern and its O value are given in Fig. 5.

Result

Random Value Simulation

Simulations with random parameter values were conducted, and the distribution of O in the results was investigated. First, 1000 parameter sets, for all of which the values of the parameters were randomly given, were generated. One hundred simulations for each parameter set were conducted to obtain the mean value of O. Figure 5 shows a histogram of the values of $\bar{O}$ for 1000 random value simulations. The range of $\bar{O}$ was $-54.06 \leq \bar{O} \leq 17.37$. Figure 5 illustrates that $\bar{O}$ is negative in most cases; only 6% of the results has positive $\bar{O}$. The results with the diagonal spatial pattern, which necessarily has positive O, are not easily obtained in Simulation B. To successfully reproduce the diagonal spatial pattern, a careful choice of parameter values is required.

Black-Box Optimization

Black-box optimizations were conducted to search for good parameter values to reproduce the diagonal spatial pattern with Simulation B. Simulated annealing was employed for the search algorithm. A mean of 100 simulation results was employed as an objective function value. Thus, the objective function was evaluated after every 100 simulation trials. Twenty black-box optimizations with different initial points were conducted, and 1000 iterations were performed for every search procedure.

Table 2 shows the top five results of 20 black-box optimization trials. The complete results are given in the Appendix. The results were organized in the descending order of objective values $\bar{O}$, and values of $\bar{O}$ in 20 searches varied over a relatively large range from -6.88 to 28.95. The best result ($\bar{O} = 28.95$) was given by $\epsilon = 0.1$ and $\delta = 1.2$. $\alpha = 0.1$, $d = 10$, $\omega = 20$, $\Delta r = 5.0$, $\hat{N} = 15$, and $g = 0.4$.

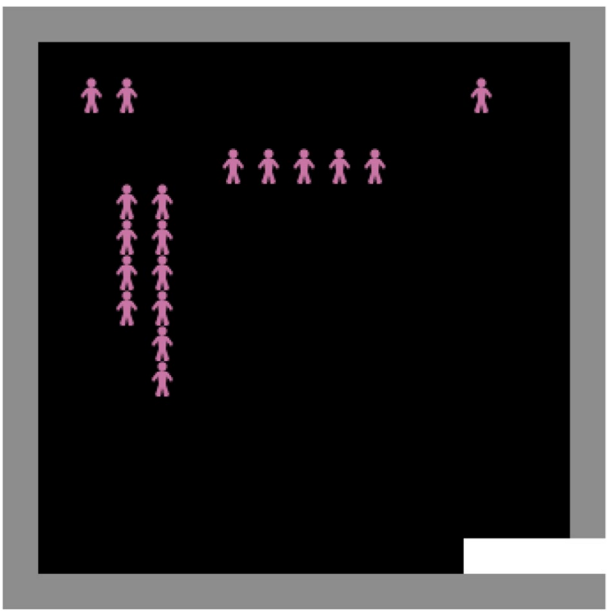

Fig. 6 Example result of Simulation B with the best parameter values ($O = 66.47$). [52]

[2] In the case of the result shown in Fig. 6, the value of O was 66.47.

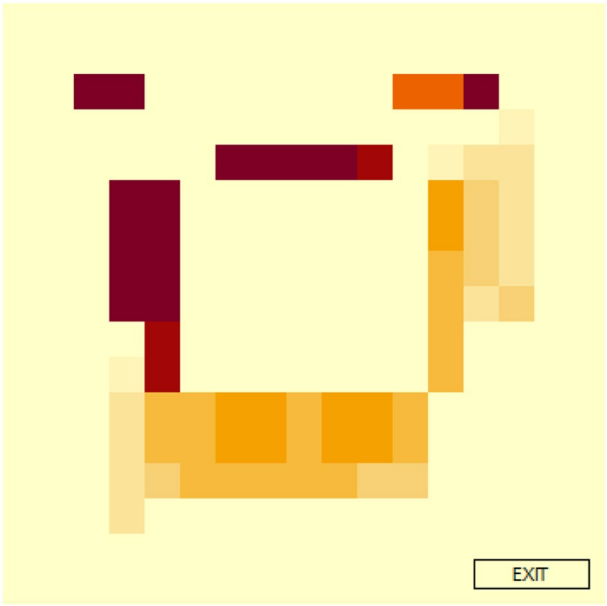

Fig. 7 Heat map of the results of 1000 simulations with the best parameter values

Result with the Best Parameter Values

An example result of Simulation B with the best parameter values above is shown in Fig. 6. As in Fig. 2, agents close to the exit selected the fleeing behavior and left the room, while the agents farther from the exit selected the dropping behavior and stayed in the room. This allowed the diagonal spatial pattern to be formed. Owing to the stochastic nature of the model, results similar to Fig. 6 were not necessarily obtained. Thus, 1000 simulations were conducted to verify the generality of the results.

Figure 7 shows a heat map of the results of 1000 simulations. Dark-colored regions indicate areas where higher concentrations of agents chose dropping behaviors. Light-colored regions signify areas where higher concentrations of agents chose to flee. Note that the logarithm of the frequency of the number of agents who remained in the room was employed to create the heat map as the frequency varies significantly.

Figure 8 depicts the histogram of the values of O for 1000 simulation results with the best parameter values.

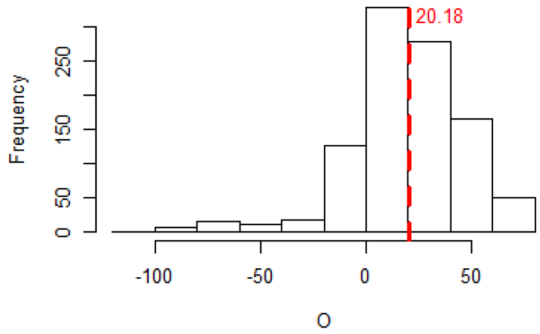

Fig. 8 Histogram of the values of O for 1000 simulations with the best parameter values. The red dashed line shows the mean of O ($\bar{O} = 20.18$)

The range of O is $-103.19 \leq O \leq 66.47$, and the mean value of O was 20.18. In most cases, the values of O were positive, implying the occurrence of the diagonal spatial pattern.

Now, it can be concluded that the evacuation behaviors captured in the video clip (Fig. 1) can be reproduced using not only Simulation A, but also in Simulation B with the best parameter values.

Parameter Analysis

By examining Table 5 carefully, it can be seen that some common parameter values lead to results similar to real situation. Table 2 summarizes parameter values and values of $\bar{O}$ for such good results. In this table, some parameters have identical or similar values, such as $\epsilon \leq 0.2$ and $d \geq 8$, and $\omega = 20$.

The statistical significance of each parameter against the objective values ($\bar{O}$) was investigated using multiple regression analysis. For this, 100 samples from the results of 1000 simulations with random parameters were randomly selected, as shown in Fig. 5, to avoid the decrease in p values because of the large data size. The results of the analyses are listed in Table 3. The top row shows the coefficient values of the parameters, and the bottom row the corresponding p values.

Table 3 reveals that d and ω are statistically significance level ($p < 0.001$). Because d is the radius and ω is the angle

Table 2 Top 5 results of black-box optimization

ϵ	δ	α	d	ω	Δr	$\hat{N}$	g	$\bar{O}$
0.1	1.2	0.1	10	20	5.0	15	0.4	28.95
0.1	0.7	0.4	10	20	2.0	1	1.5	27.76
0.1	1.1	0.8	8	20	5.0	2	1.4	26.64
0.2	0.6	0.6	9	20	2.5	7	1.4	26.23
0.1	1.0	0.2	10	20	1.5	20	0.2	26.22

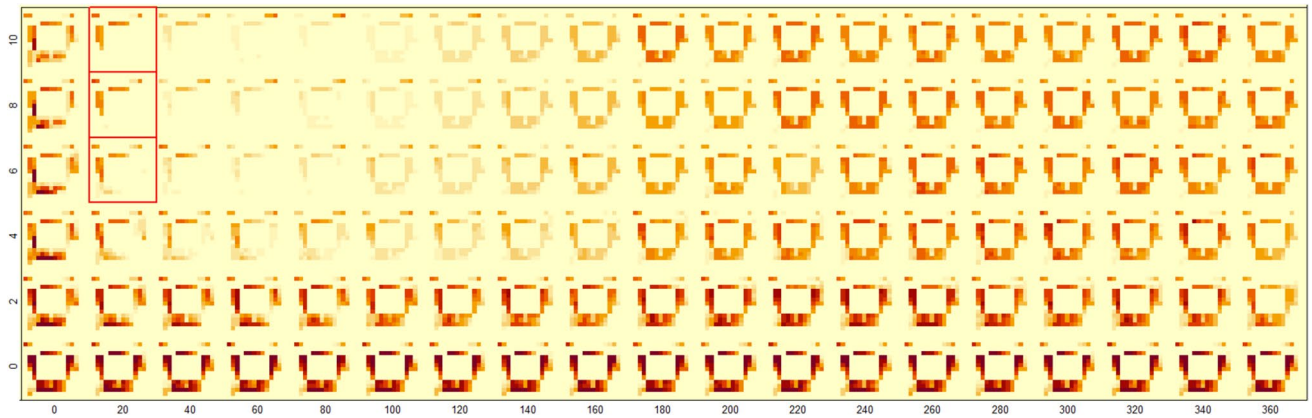

Fig. 9 Results of sensitivity analysis for d and ω. The rows show d and the columns show ω. Each cell shows the heat map of 100 simulations. Cells with red square frames refer to the results for $\bar{O} > 10$. [52]

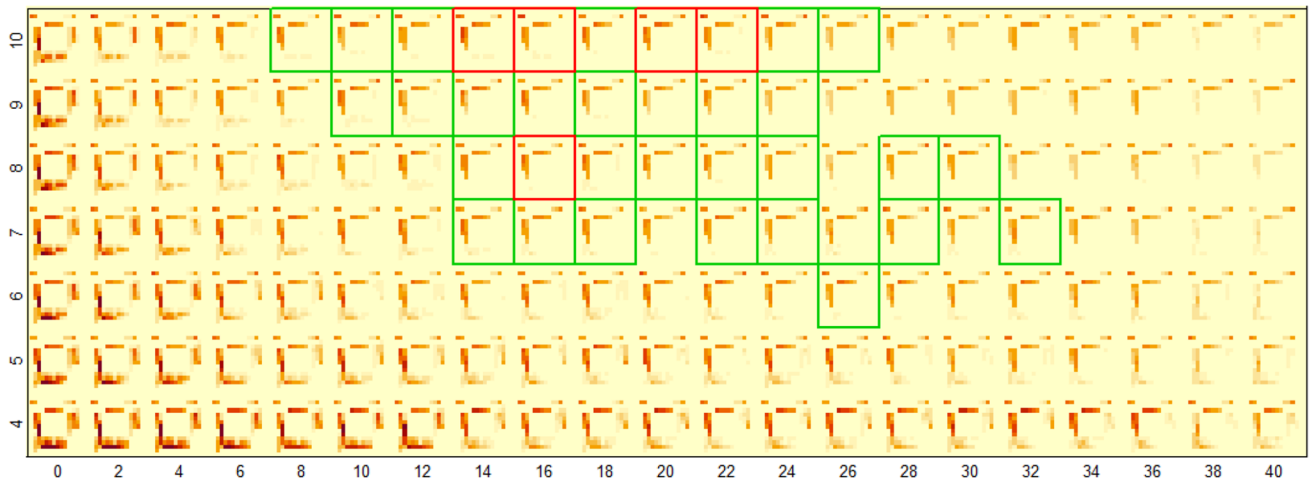

Fig. 10 Results of the focused analysis of Fig. 9. The ranges of ω and d are enlarged to $0 \leq \omega \leq 40$, and $4 \leq d \leq 10$, respectively. The cells with green frames are referred to as the results for $\bar{O} > 15$ (red frames) and $\bar{O} > 20$

of the fan of the visual field of an agent, the result implies that the visual field of an agent significantly affects the simulation results. Furthermore, ϵ is also statistically significant ($p < 0.01$).

Then, a sensitivity analysis to examine the effects of parameters d and ω on the occurrence of the diagonal spatial pattern was conducted by varying d from 0 to 10, and ω from 0 to 360. A total of 100 simulations were conducted for each combination of d and ω. The coordinates of all remaining agents at the end of simulations were recorded; these coordinates were represented as a heat map of the analysis results.

Figure 9 illustrates the heat maps of the results of simulations with all combinations of d and ω. The rows in the figure represent the values of d, and the columns represent the values of ω. Each cell in the figure represents the positions of the remaining agents at the end of a simulation. The dark color shows a higher frequency and the light color shows a lower frequency of the remaining agents.

Figure 9 reveals that most combinations of d and ω values produce a spatial pattern dissimilar to the one captured in the video clip. Only a few combinations, found at the upper left in the figure, produced the diagonal spatial pattern. The red square frames in the figure refer to combinations of d and ω with $\bar{O} > 10$. This reveals that only parameters with $d \geq 8$, and $\omega = 20$ will lead to the diagonal spatial pattern. These results are in agreement with the results in Table 2.

A focused analysis for ω and d was conducted to examine the optimal parameter space in detail. A total of 100 simulations were carried out for all the combinations with $\omega = \{0, 2, 4, 6, 8, 10, 12, 14, 16, 18, 20, 22, 24, 26, 28, 30, 32, 34, 36, 38, 40\}$ and $d = \{4, 5, 6, 7, 8, 9, \text{and } 10\}$, and the results are shown in Fig. 10. In this figure, the results with $\bar{O} > 15$

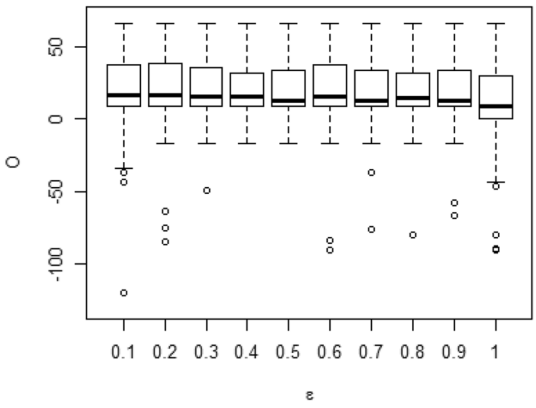

Fig. 11 Results of sensitivity analysis for ϵ. *Y*-axis depicts the values of O. [52]

are indicated by green frames, and $\bar{O} > 20$, red frames. The best result was obtained when $\omega = 14$ and $d = 10$.

A sensitivity analysis for ϵ, which is a transition probability of $X = 1$ to $X = 0$, and another significant parameter mentioned above, was also conducted with values ranging from 0.1 to 1.0. With fixing d and ω to 10 and 20, respectively, 100 simulations were conducted by varying values of ϵ. The results are presented in Box-and-Whisker diagrams in Fig. 11. The x-axis represents the value of ϵ, and the y-axis, O. Furthermore, the x-axis represents the values of ϵ and the y-axis O. The figure illustrates that the values of ϵ do not affect simulation results much as long as the values of d and ω are fixed within a certain range, implying that the transition probability of random selection ($X = 1$) to herd behavior ($X = 0$) is unrelated to the occurrence of a diagonal spatial pattern.

Tunnel Vision Hypothesis

This study demonstrated that the simulation with realistic settings (Simulation B) could reproduce the diagonal spatial pattern of evacuees' decisions to either flee or drop the video clip captured during the Great East Japan Earthquake. The study also demonstrated this in Simulation A. However, this is only true within a limited range of parameter values in Simulation B.

Parameter values that can reproduce the diagonal spatial pattern were explored using a black-box optimization technique. Several sets of parameter values yielding the diagonal spatial pattern (e.g., $d \geq 8$ and $14 \leq \omega \leq 22$) were found and, in these sets, some parameters with similar or identical values were observed. The multiple regression analysis revealed that parameters d and ω were statistically significant; the occurrence of the diagonal spatial pattern is therefore affected by these two parameters. The sensitivity analysis for d and ω illustrate that the limited ranges of parameter values lead to the diagonal spatial pattern. This highlighted that the diagonal spatial pattern is scarcely obtained outside the specified ranges of these two parameters. The diagonal spatial pattern was not obtained using the parameter settings employed in simulation A (i.e., $d = 5$ and $\omega = 120$).

Both d and ω refer to the definition of an agent's visual field. The visual field of an agent is assumed to be fan shaped with radius d and angle ω in the heading direction of the agent. A red fan with $d = 10$ and $\omega = 20$, as shown in Fig. 4, depicts the visual field of the red agent in the upper left corner of the figure. This definition can be considered narrow and lengthy, because the size of the space was only 15×15 units. The visual field of an agent will affect the evacuation behavior of the agent when the agent experiences herd behaviors. The analysis above leads to the following hypothesis.

Tunnel Vision Hypothesis During evacuations, the visual field of an evacuee is narrowed to a range of about 20° with a relatively long distance.

Comparative Analysis Between Simulations A and B

One may criticize our results, saying that they rely upon only one instance of objective data (in this case, a video clip captured during the Great East Japan Earthquake), which was merely one exceptional case. However, this criticism is invalid, because the study of Simulation A reveals that

Table 3 Result of multiple regression analysis

	ϵ	δ	α	d	ω	Δr
Coef	7.68	3.21	1.42	1.50	− 0.06	1.18
p val	0.01	0.06	0.36	0.00	0.00	0.05
	$\hat{N}$	g				
Coef	0.12	− 1.81				
p val	0.50	0.35				

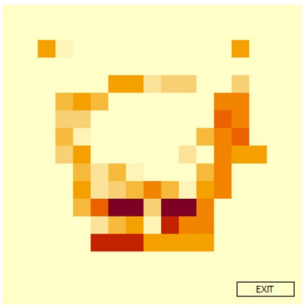

Fig. 12 The results of Simulation B without physical constraints

the diagonal spatial pattern would occur frequently. Neither the conditions in Simulation A nor the evacuation decision model involve any factor that can make an arbitrary decision; only primitive mechanisms are incorporated in Simulation A. Therefore, the occurrence of the diagonal spatial pattern may even be considered a physical phenomenon. In contrast, the diagonal spatial pattern is hardly obtained in Simulation B. Examining which condition in Simulation B causes difficulty in obtaining the diagonal spatial pattern is intriguing and crucial. This is because the tunnel vision hypothesis is mainly supported by the difficulty in obtaining the diagonal spatial pattern in Simulation B.

First, the effect of the physical constraints that were disregarded in Simulation A was investigated. An agent in a constraint-free setting can move toward the only exit directly, and can do so even if other agents are in the way of the exit. Meanwhile, the actual movements of the agents in Simulation B were constrained.

A total of 300 simulations with the settings of Simulation B, without the physical constraints, were conducted. This meant that the agents in this setting could move to the exit even if the other agents stayed between them and the exit. The parameter values employed in this simulation are equivalent to those used in Fig. 7. The result of the simulations is illustrated in the heat map in Fig. 12. The dark color in the heat map depicts a region with a higher frequency of agents dropping. Correspondingly, a light color indicates a lower frequency. The diagonal spatial pattern was hardly obtained in this setting.

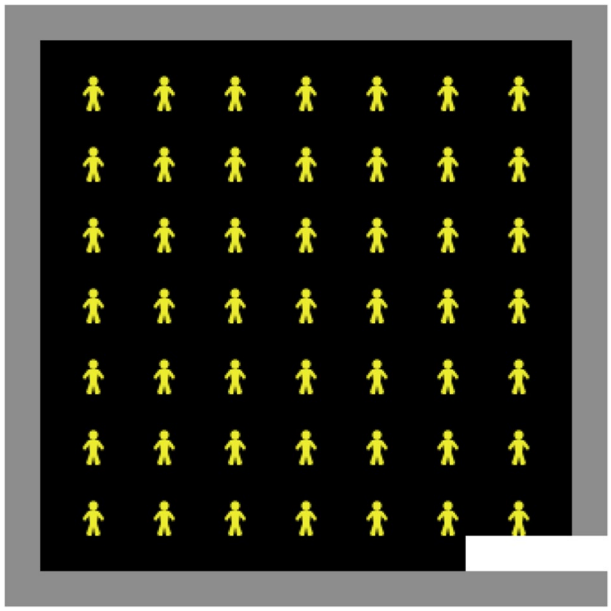

Fig. 14 Initial positions of 49 agents arranged in 7 by 7

A sensitivity analysis for parameters d and ω in this setting was also conducted. The results of the analysis are presented in the heat maps in Fig. 13. The diagonal spatial pattern is unseen in any combination of d and ω in Fig. 13. Unlike the original Simulation B where only a few combinations of d and ω leads to a diagonal spatial pattern, and the absence of physical constraints in this setting negatively affects the occurrence of the diagonal spatial pattern. To create a diagonal spatial pattern, it was necessary to consider the physical constraints in Simulation B.

Fig. 13 The results of sensitivity analysis for d and ω for the results of 100 simulations of Simulation B without considering physical constraints

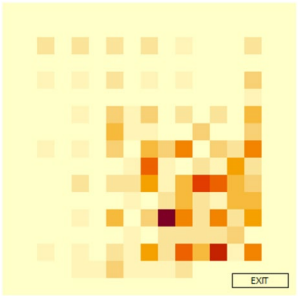

Fig. 15 The results of Simulation B with a uniform initial arrangement of agents

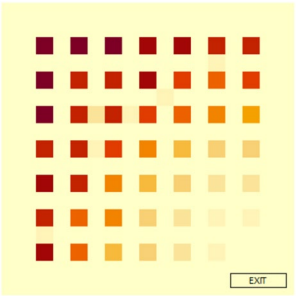

Fig. 17 The results of Simulation B with a uniform initial arrangement of agents for the best parameter values

Next, the different initial arrangements of the agents were investigated. A total of 300 simulations using 49 agents, initially uniformly arranged at 7×7, as shown in Fig. 14,were conducted. The results are presented in the heat map in Fig. 15. The darker color depicts regions with a higher frequency of the agents who opted to drop, while the lighter color depicts a lower frequency. The figure clearly shows that the diagonal spatial pattern did not emerge in this setting. The result contradicts the expectation that relaxing constraints would induce the diagonal spatial pattern more frequently. Then, sensitivity analysis for d and ω with this setting was conducted. Figure 16 depicts the analysis results. Here, the diagonal spatial pattern emerges in some combinations of d and ω, for example, $d = 4, \omega = 240$, and $d = 2, \omega = 360$, showing that the diagonal spatial pattern could be obtained depending on parameter values in the uniform initial arrangement.

Black-box optimizations starting from different initial points were conducted to explore a set of parameter values to reproduce the diagonal spatial pattern in this initial arrangement. The black-box optimizations were performed ten times with varying initial points, and each optimization contained 100 iterations. The best result was given by $\epsilon = 0.4, \delta = 0.9, \alpha = 2, d = 3, \omega = 240, \Delta r = 0.5, \hat{N} = 7$, and $g = 0.9$. Figure 17 depicts the heat map of 300 results with these parameters. The dark and light color convey a higher frequency of dropping and fleeing agents in this area. Furthermore, in this figure, the area close to the exit is light, and the area farthest from the exit is dark. This means that agents close to the exit opted for fleeing behavior and left. Meanwhile, the agents farthest from the exit pursued the dropping behavior and remained. This implies the occurrence of the diagonal spatial pattern. Furthermore, a sensitivity analysis for d and ω was conducted, and the result is presented in Fig. 18. In this figure, the diagonal spatial pattern can be observed in several combinations of d and ω. However, these results did not improve those in Fig. 16 significantly.

Influence Analysis

In herd behavior, the decision of an agent is determined by other agents' decisions within the visual field of that agent. Algorithm 1 describes this process; the other agents that affected the agent's current decision were stored in E_i^d or E_i^f —lines 6 or 9 in algorithm 1, respectively.

An influence graph is a tuple, $(\mathcal{G}, \psi)$, where $\mathcal{G} = (A, \mathcal{E})$ is a labeled directed graph, A is a set of vertices or agents, $\mathcal{E}$ is a set of directed edges and $\psi : \mathcal{E} \rightarrow \{\text{flee}, \text{drop}\}$ is a labeling function designating fleeing or dropping behaviors. An ordered pair $(a_i, a_j) \in \mathcal{E}$ refers to the influence of

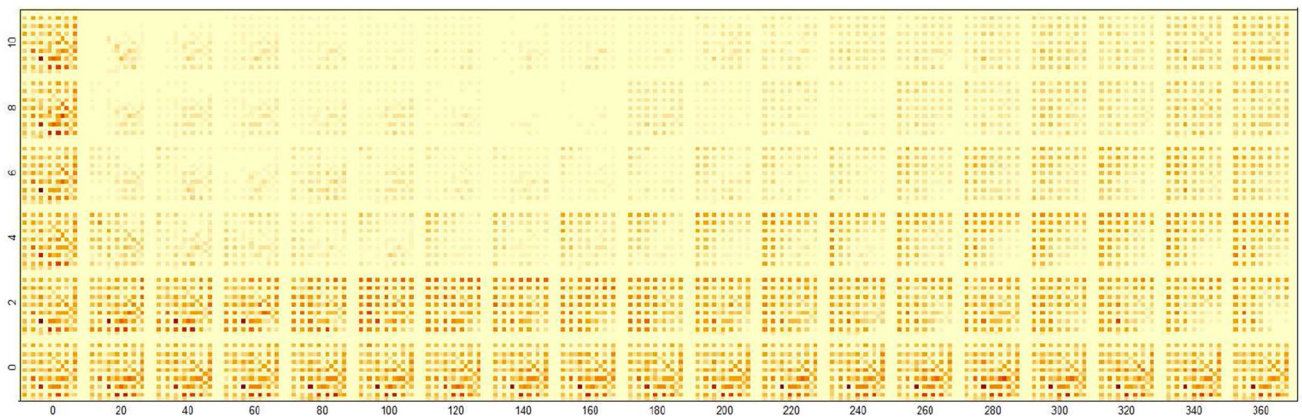

Fig. 16 Sensitivity analysis of 100 simulations of Simulation B with a uniform initial arrangement of agents

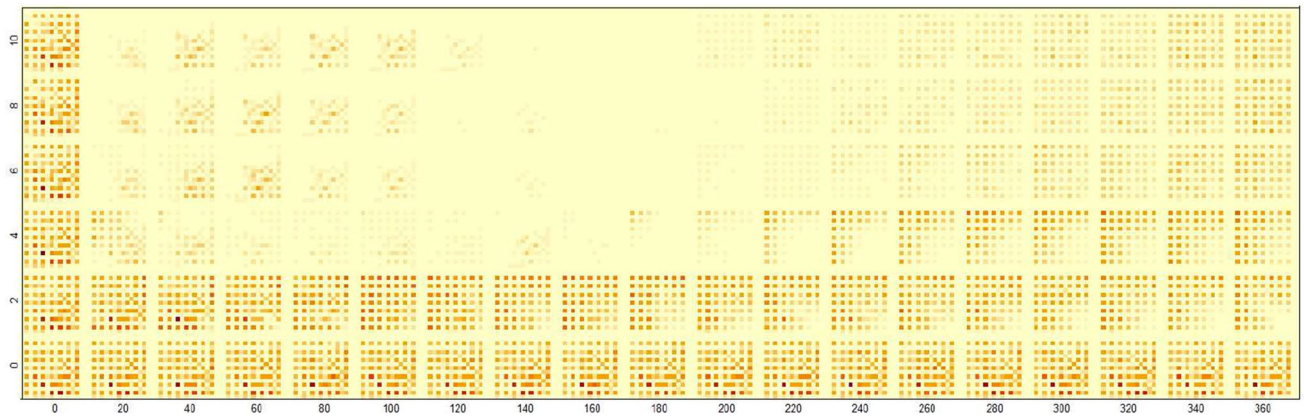

Fig. 18 Sensitivity analysis of 100 simulations of Simulation B with a uniform initial arrangement of agents for the best parameter values

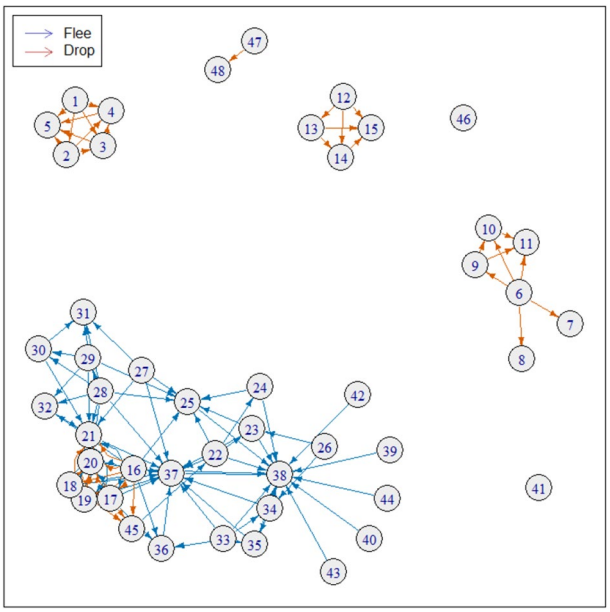

Fig. 19 The influence graph of the simulation result in Fig. 6

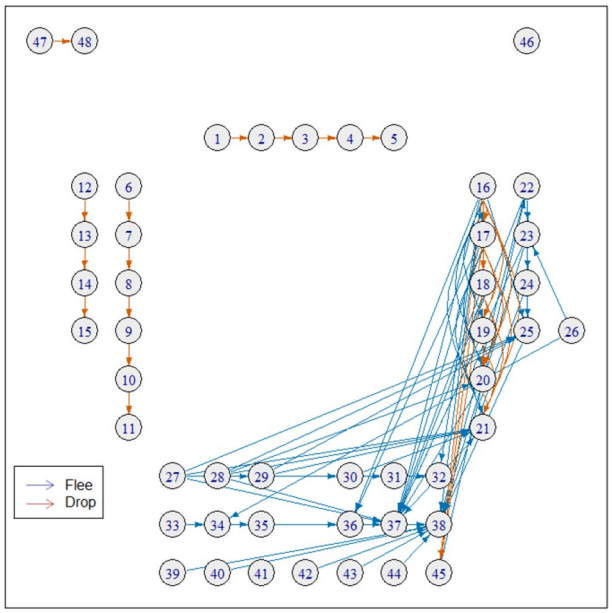

Fig. 20 The influence graph of Fig. 19 embedded in the initial layout

$a_j \in \{E_i^d \cup E_i^f\}$ to a_i. Figure 19 depicts an example of the influence graph in the simulation in Figs. 6, and 20 shows the same graph embedded in the initial layout. A blue arrow represents the influence of fleeing behavior, while a red arrow represents the influence of dropping behavior. The head of an arrow designates the affecting agent, and the tail designates the affected agent. Figure 19 reveals that there are four types of agents that are affecting/affected by:

1. Both fleeing and dropping behaviors: 16, 17, 18, 19, 20, 21, and 45.
2. Dropping behavior: 1, 2, 3, 4, 5, 6, 7, 8, 9, 10, 11, 12, 13, 14, 15, 47, and 48.
3. Fleeing behavior: 22, 23, 24, 25, 26, 27, 28, 29, 30, 31, 32, 33, 34, 35, 36, 37, 38, 39, 40, 42, 43, and 44.
4. None: 41 and 46.

Agents in types 1 and 3 form one big subgraph; these agents eventually selected fleeing behavior and left the room. In contrast, agents in type 2 form four small graphs; these agents selected dropping behavior and remained in the room. Figure 20 reveals that each group of agents in these small graphs aligns in the same row or column in the initial arrangement. For example, agents 12, 13, 14, and 15 form a

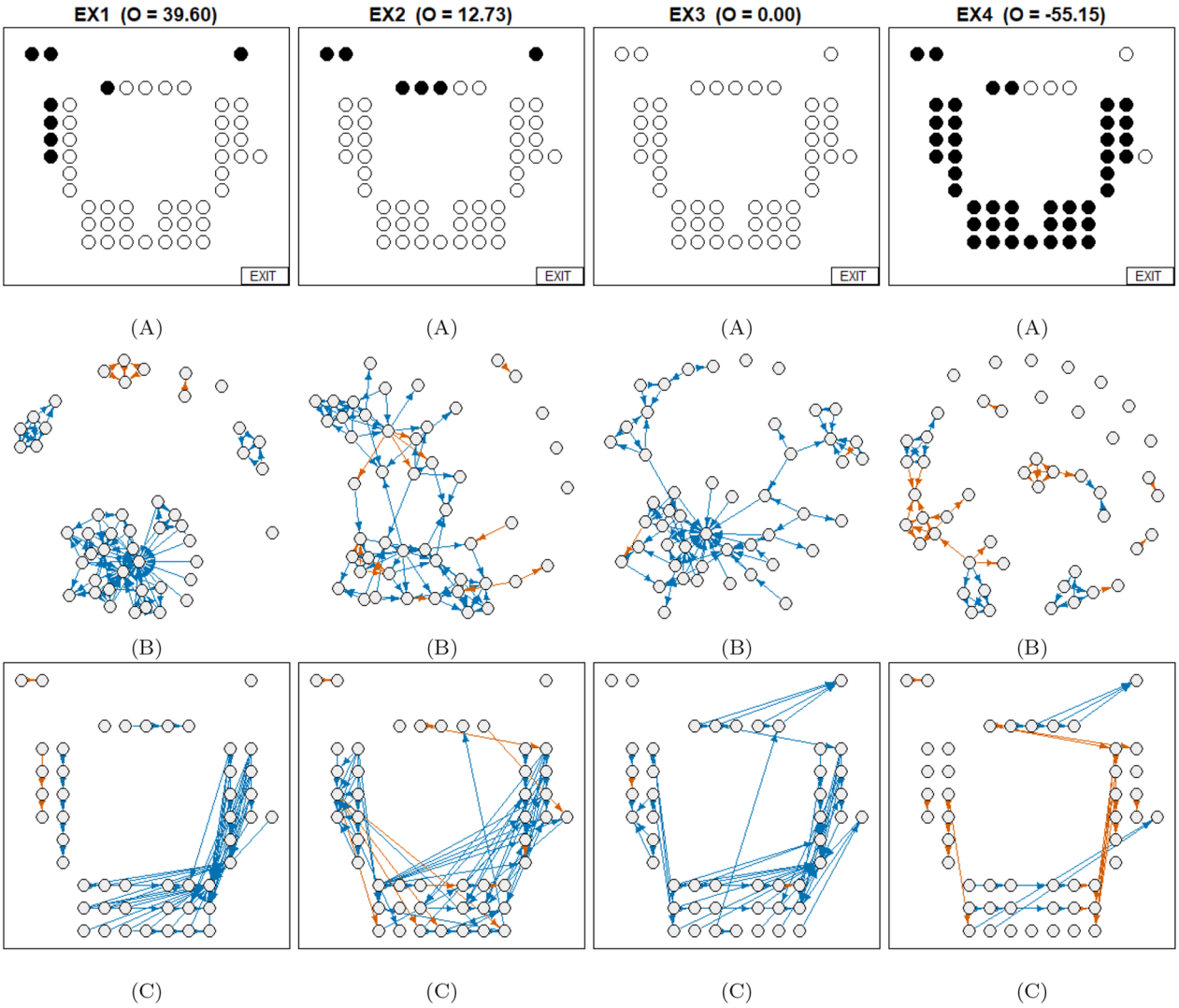

Fig. 21 Four examples (EX1–4) of final agents' positions (**a**), corresponding influence graphs (**b**), and influence graphs embedded in the initial layout (**c**). In (**a**), a black circle depicts an agent selecting dropping behavior and remaining in the room. *O* values are indicated at the top of (**a**)

line along the left edge of the room, implying that a narrow and long visual field of agents may cause these groupings.

Figure 21 presents four examples of simulation results (EX1 to 4): (A) depicts the agents' final decisions at the location of their initial positions. (B) Corresponding influence graphs. (C) Influence graphs embedded in initial layout. The *O* value of each result is given at the top of (A).

These figures reveal that the more an influence graph was divided into subgraphs, the more dropping agents remained in the room. For example, the influence graph of EX4 consists of many subgraphs and isolated nodes, and the final layout of EX4 contains many dropping agents (25). In contrast, the final layout of EX3 contains no dropping agent, and most nodes in the influence diagram of EX3 belong to one big subgraph, except two isolated nodes. The influence of dropping behavior within big subgraphs, even if observed, was overwhelmed by the influence of fleeing behavior. These results imply that most agents select fleeing behaviors and leave the room if the effects of fleeing behaviors propagate over them. However, more agents selecting dropping behavior remained in the room if the influences of the agents' decisions were interfered with and, therefore, failed to spread within limited ranges.

Figure 22 illustrates affecting and affected agents for both fleeing and dropping behavior in association with their initial positions. The first and second figures depict affecting and affected agents in fleeing behavior; the third and fourth figures depict affecting and affected agents in dropping behavior. The affecting and affected agents are represented in red and blue, respectively. The darker the colors are, the stronger

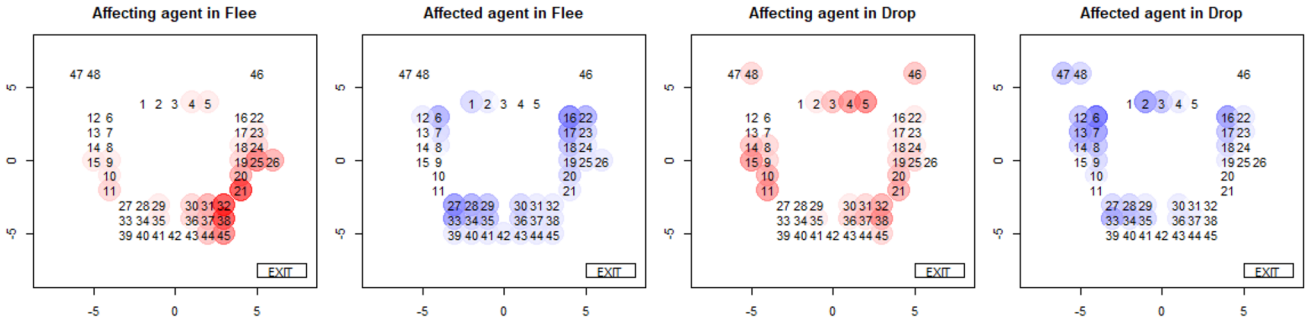

Fig. 22 Affecting and affected agents in initial positions

the influences. These figures show that the agents' specific positions in the initial layout have unique effects on fleeing and dropping behaviors. For example, the positions close to the exit strongly affect other agents, especially regarding fleeing behaviors. Conversely, the positions at the corner opposite the exit are strongly affected by other agents' dropping behaviors.

A total of 100 simulations with identical settings in Fig. 6 were conducted, and the results were converted into two groups based on O values. C^+ represents the group of results with $O \geq 25$,C^-, and $O < 25$. The diagonal spatial pattern can be expressed as obtained in C^+ but not in C^-. Paired t tests for C^+ and C^-, with several criteria for each agent were conducted to investigate the statistically significant differences. The criteria analyzed in the t tests are as follows:

– Agent parameter

1. Response threshold (θ_i)
2. Risk sensitivity (μ_i)

– Node centrality in $\mathcal{G}$

1. Degree centrality (DG)
2. Page-rank centrality (PR)
3. Betweenness centrality (BW)

Table 4 p values in t test between C^+ and C^- ($O = 25$)

$\lvert C^+\rvert$	θ_i	μ_i	DG	PR	BW	RS	TIME
55	0.51	0.66	0.43	1	0.46	0.00	0.09
49	0.04	0.65	0.05	1	0.71	0.26	0.00
43	0.22	0.98	0.09	1	0.00	0.00	0.02
47	0.86	0.77	0.62	1	0.23	0.00	0.53
43	0.54	0.70	0.61	1	0.00	0.00	0.14
44	0.90	0.53	0.12	1	0.00	0.00	0.00
52	0.33	0.42	0.18	1	0.77	0.00	0.25
53	0.59	0.44	0.42	1	0.00	0.00	0.61
44	0.19	0.91	0.06	1	0.00	0.00	0.00
53	0.22	0.93	0.87	1	0.82	0.00	0.03

– Dynamics in evacuation

1. Ratio of random selection period ($X = 1$) during the evacuation (RS)
2. Time duration until the first action (fleeing or dropping) (TIME).

The above t test was conducted ten times, because the results were not perfectly stable.

Table 4 summarizes the p values of the ten t tests with respect to the above criteria. If the difference between the means of C^+ and C^- are statistically significant ($p < 0.05$); the corresponding cells in the table are highlighted in blue. In this table, it can be observed that the results of the t test were almost statistically significant in RS. The results of half tests were statistically significance, but the other half were not deemed to be so in BW or TIME. However, the results were not statistically significant in θ_i, μ_i, DG, and PR. Using this analysis, the following were concluded:

1. The occurrence of the diagonal spatial pattern is independent of the individual differences of the agents (θ_i and μ_i).
2. In graph centrality analysis, the betweenness centrality (BW) may have some effect on the occurrence of the diagonal spatial pattern. However, the degree (DG) and page-rank (PR) centralities do not.
3. The ratio of the random selection period by the total evacuation time (RS) will affect the occurrence of the diagonal spatial pattern, and time duration until the first action (TIME) may also have some effects.

Discussion

In the analysis of the diagonal spatial pattern, which was found thorough the video clip analysis captured during the Great East Japan Earthquake, the tunnel vision hypothesis was proposed. This can be paraphrased that the visual field

of an evacuee narrows to about 20° with a relatively long distance during an evacuation. This hypothesis is worth studying, because most studies regarding disaster evacuations assume a wider visual field for an agent. Prior to the present study, simulations and experiments that included narrower visual fields were yet to be conducted extensively. As the difference between the tunnel vision hypothesis and the assumptions in the conventional studies is significant, the study of the tunnel vision hypothesis may lead to unexpected results in evacuation studies. This could possibly alter evacuation protocol designs that are currently considered optimized.

The diagonal spatial pattern in earthquake evacuations (i.e., the decision between fleeing and dropping is determined by the distance from the exit) is a unique evacuation behavior yet to be reported in the literature, to the best of our knowledge. Moreover, this video is unique. Thus, if the diagonal spatial pattern could be considered a mere exception, the generality of this phenomenon might be doubtful. However, our previous study examined the generalizability of the occurrence of the diagonal spatial pattern and revealed that this pattern occurs frequently in general [51]. The result of the temporal analysis of evacuation behaviors of 48 people discussed in [51] is coherent with [17], which is the cumulative curve of evacuees over evacuation time is convex. This fact additionally supports our result. This study is essentially a parameter analysis of the evacuation decision model, assuming the model is correct. The out-of-sample test of the model was not conducted in this study. More objective data about evacuation behaviors in an earthquake are desirable.

Using comparative analysis, the effects of several conditions upon the diagonal spatial pattern in Simulation B were investigated. Although the results were not as comprehensive as anticipated, some implications could be derived. The diagonal spatial pattern emerged if, as in Simulation A, agents were uniformly arranged around the room (Fig. 14). However, this was not the case when the agents were arranged in a square, as they were in the video (Fig. 3). The fact that the diagonal spatial pattern could reoccur upon the implementation of physical constraints was found. In summary, both the uniform arrangement of and the application of physical constraints upon agents resulted in a higher occurrence of the diagonal spatial pattern. Conversely, a square arrangement resulted in a lower occurrence. In the uniform arrangement, as well as in Simulation A, all fleeing agents move directly toward the exit. Therefore, numerous agents close to the exit are subject to these agents' effects. By contrast, in the square arrangement, the number of agents close to the exit was small. A few agents are positioned in the trajectories of the other fleeing agents. Thus, the influence of fleeing agents on herd behavior was not significant. This is particularly true if the visual field of the agent is narrow. In this case, a diagonal spatial pattern hardly emerges. However, if constraints on the physical movements of the agents are considered, as demonstrated in Fig. 4, then the agents along the right and bottom edges are affected by fleeing agents. In this case, the diagonal spatial pattern is more likely to be obtained.

The influences on agents during herd behaviors were investigated in the influence analysis. The influence analysis graphs revealed that numerous dropping agents would remain in the room and likely form the diagonal spatial pattern if the influence graph was deconstructed into several subgraphs. The analysis also revealed that the initial position of an agent was crucial; both the affecting and affected agents of fleeing and dropping behaviors depended immensely on their initial location in relation to the exit. Furthermore, the analysis of two groups (C^+ and C^-) revealed some intriguing results:

1. Individual properties (θ_i and μ_i) are independent of the occurrence of the diagonal spatial pattern.
2. The agents connecting two subgroups are more critical than influential agents.
3. The individual dynamics during evacuations, for example, the ratio of self-decided behaviors ($X = 1$) over herd behavior ($X = 0$), will significantly affect crowd behaviors.

One of the most unexpected results in the video analysis is the fact that many evacuees exhibited fleeing behavior. This was unexpected, because it is widely known that fleeing during an earthquake is dangerous and not recommended. This is the case in Japan and other countries. Safety education and trainings take place frequently, and drop cover hold on actions is recommended in all these programs. Fleeing behaviors, however, are not recommended nor taught in these programs [26]. The result that individual properties did not affect the crowd's evacuation behaviors may suggest that the effectiveness of safety behavior education at the individual level is limited. Furthermore, the importance of agents' initial positions, as well as results 2 and 3 above, implies that there are new approaches that can unconsciously intervene during evacuations and alter agents' behaviors. One of these novel approaches are environment designs that use nudge techniques [30].

The results of this study do not deny the first theory in the Diagonal Spatial Pattern section; rather, I consider it natural

for people close to the exit to select intentionally the option to escape. Assuming the distance threshold is 12 units, simulations with the first theory will have $\bar{O} = 62.23$, which is significantly better than our result ($\bar{O} = 21.18$ in Fig. 8). This is not surprising, because the first theory is deterministic and always reproduces the diagonal spatial pattern as long as the threshold is properly given. In reality, I believe that both theories will hold simultaneously, and the evacuation process of humans will be a complex mixture of higher and lower level cognitions.

Conclusion

Through the analysis of the video clip captured during the Great East Japan Earthquake, the evacuation behaviors of people in the video were reproduced by simulations employing the evacuation decision model with realistic settings. As a sequel to the simulations, the tunnel vision hypothesis (i.e., the visual field of an evacuee narrowed to about 20° with length distance) was proposed. The conditions that produce the diagonal spatial pattern were analyzed, and results that both the uniform arrangement of and the application of physical constraints upon agents led to a high occurrence of the diagonal spatial pattern, but a square arrangement led to a lower occurrence were found. Furthermore, the influence analysis revealed that the initial positions and the individual dynamics during evacuations affect the crowd evacuation behaviors rather than the individual differences.

Appendix

The following table shows the results of the parameter searches using black-box simulation in descending order of $\bar{O}$. Searches were conducted 20 times with different initial points.

Table 5 Results of black-box optimization

ϵ	δ	α	d	ω	Δr	$\hat{N}$	g	$\bar{O}$
0.1	1.2	0.1	10	20	5.0	15	0.4	28.95
0.1	0.7	0.4	10	20	2.0	1	1.5	27.76
0.1	1.1	0.8	8	20	5.0	2	1.4	26.64
0.2	0.6	0.6	9	20	2.5	7	1.4	26.23
0.1	1.0	0.2	10	20	1.5	20	0.2	26.22
0.2	1.9	1.9	10	10	1.5	6	1.3	25.96
0.3	1.8	0.9	6	20	4.5	19	0.3	23.43
1.0	0.5	0.7	10	10	4.5	13	1.6	22.27
0.6	0.6	1.4	7	10	5.0	4	1.9	22.16
0.1	1.2	0.9	7	20	4.0	2	1.1	22.04
0.3	1.9	0.7	6	20	3.0	15	1.1	22.01
0.7	0.3	0.7	10	10	2.5	2	1.4	21.96
0.4	0.7	0.0	6	20	1.5	4	1.0	21.92
0.7	0.5	1.2	3	70	3.5	16	1.0	15.76
1.0	1.7	1.6	3	70	3.0	1	1.4	15.59
0.8	0.6	0.2	3	80	1.0	7	0.4	12.91
0.6	1.6	1.2	3	70	3.5	1	0.5	12.87
0.8	1.8	1.4	3	70	3.0	1	0.1	12.03
0.8	0.2	1.8	4	360	4.0	11	0.4	− 5.95
0.4	1.7	0.0	5	330	2.0	10	0.8	− 6.88

Acknowledgements I would like to express my gratitude to Mr. Kei Marukawa for his comments and suggestions. I would also like to thank Editage (www.editage.com) for the English language editing.

Declarations

Conflict of interest The author is an employee of Secom Co., Ltd.

References

1. Altshuler E, Ramos O, Nuñez Y, Fernańdez J, Batista-Leyva AJ, Noda C. Symmetry breaking in escaping ants. Am Nat. 2005;166(6):643–9.
2. Bae YH, Kim YC, Oh RS, Son JY, Hong WH, Choi JH. Gaze point in the evacuation drills: analysis of eye movement at the indoor wayfinding. Sustainability. 2020;12(2902):1–14.
3. Berton F, Hoyet L, Olivier AH, Bruneau J, Le Meur O, Pettre J. Eye-gaze activity in crowds: impact of virtual reality and density. In: 2020 IEEE conference on virtual reality and 3D user interfaces (VR); 2020. p. 322–31. https://doi.org/10.1109/VR46266.2020.00052.
4. Bonabeau E, Sobkowski A, Theraulaz G, Deneubourg JL. Adaptive task allocation inspired by a model of division of labor in social insects. In: Proceeding of biocomputing and emergent computation; 1997. p. 36–45.
5. Bonabeau E, Theraulaz G, Deneubourg JL. Quantitative study of the fixed threshold model for the regulation of division of labour in insect societies. Proc R Soc B. 1996;263(1376):1565–9.
6. Burke A, Heuer F, Reisberg D. Remembering emotional events. Mem Cognit. 1992;20:277–90.
7. Chan HS, Courtney AJ. Effects of cognitive foveal load on a peripheral single-target detection task. Percept Motor Skills. 1993;77(2):515–33. https://doi.org/10.2466/pms.1993.77.2.515.
8. Christianson SC. Emotional stress and eyewitness memory: a critical review. Psychol Bull. 1992;112(3):284–309.
9. Christianson SC, Loftus EF. Memory for traumatic events. Appl Cognit Psychol. 1987;1(4):225–39. https://doi.org/10.1002/acp.2350010402.
10. Crundall D, Underwood G, Chapman P. Driving experience and the functional field of view. Perception. 1999;28(9):1075–87. https://doi.org/10.1068/p2894.
11. Ding N, Chen T, Liu Y. Evacuation guidance design: an experimental study based on eye tracking devices. Collect Dyn. 2020. https://doi.org/10.17815/CD.2020.52.
12. D'Orazio M, Spalazzi L, Quagliarini E, Bernardini G. Agent-based model for earthquake pedestrians' evacuation in urban outdoor scenarios: behavioural patterns definition and evacuation paths choice. Saf Sci. 2014;62:450–65. https://doi.org/10.1016/j.ssci.2013.09.014.
13. Drury J, Brown R, González R, Miranda D. Emergent social identity and observing social support predict social support provided by survivors in a disaster: solidarity in the 2010 Chile earthquake. Eur J Soc Psychol. 2015;46(2):209–23. https://doi.org/10.1002/ejsp.2146.
14. Filippidis L, Galea E, Gwynne S, Lawrence P. Representing the influence of signage on evacuation behavior within an evacuation model. J Fire Protect Eng. 2006;16:37–73. https://doi.org/10.1177/1042391506054298.
15. Galea RE, Xie H, Lawrence JP. Experimental and survey studies on the effectiveness of dynamic signage systems. Fire Saf Sci. 2014;11:1129–43.
16. Garcimartín A, Zuriguel I, Pastor J, Martín-Gómez C, Parisi, D. Experimental evidence of the "faster is slower" effect. Transp Res Procedia. 2014;2:760 – 767. https://doi.org/10.1016/j.trpro.2014.09.085. In: The conference on pedestrian and evacuation dynamics 2014 (PED 2014), 22–24 October 2014, Delft, The Netherlands
17. Gu Z, Liu Z, Shiwakoti N, Yang M. Video-based analysis of school students' emergency evacuation behavior in earthquakes. Int J Disaster Risk Reduct. 2016;18:1–11. https://doi.org/10.1016/j.ijdrr.2016.05.008.
18. Haghani M. Empirical methods in pedestrian, crowd and evacuation dynamics: part i. experimental methods and emerging topics. Saf Sci. 2020;129:104743. https://doi.org/10.1016/j.ssci.2020.104743.
19. Haghani M. Empirical methods in pedestrian, crowd and evacuation dynamics: part ii. Field methods and controversial topics. Saf Sci. 2020;129:104760. https://doi.org/10.1016/j.ssci.2020.104760.
20. Haghani M, Sarvi M, Shahhoseini Z, Bolts M. How simple hypothetical-choice experiments can be utilized to learn humans' navigational escape decisions in emergencies. PLoS One. 2016;11(11):e0166908. https://doi.org/10.1371/journal.pone.0166908.
21. Harada Y, Mitsudo H, Ohyama J. The effect of unusualness on the functional field of view in unsafe scenes. Vis Cognit. 2020;28:1–13. https://doi.org/10.1080/13506285.2020.1718817.
22. Helbing D, Farkas I, Vicsek T. Simulating dynamical features of escape panic. Nature. 2000;407(28):487–90.
23. Holmes D, Cohen K, Haith M, Morrison F. Peripheral visual processing. Percept Psychophys. 1977;22:571–7. https://doi.org/10.3758/BF03198765.
24. Jarmasz J, Herdman C, Jóhannsdóttir KR. Object-based attention and cognitive tunneling. J Exp Psychol Appl. 2005;11(1):3–12.
25. Ji Q, Xin C, Tang S, Huang J. Symmetry associated with symmetry break: revisiting ants and humans escaping from multiple-exit rooms. Phys A. 2017. https://doi.org/10.1016/j.physa.2017.11.024.
26. Komen A. New Zealand ShakeOut: more than 1.3 million people in New Zealand participate in a drop, cover and hold earthquake drill. Aust J Emerg Manag. 2012;27(4):21–4.
27. Latané B, Darley JM. Group inhibition of bystander intervention in emergencies. J Pers Soc Psychol. 1968;10(3):215–21.
28. Li X, Guo F, Kuang H, Geng Z, Fan Y. An extended cost potential field cellular automaton model for pedestrian evacuation considering the restriction of visual field. Phys A Stat Mech Appl. 2019;515:47–56. https://doi.org/10.1016/j.physa.2018.09.145.
29. Li Y, Zhang P, Zhang H. Study on the location of building evacuation indicators based on eye tracking. In: Proceedings of the 3rd ACM SIGSPATIAL workshop on emergency management using, EM-GIS' 17. New York, NY, USA: Association for Computing Machinery; 2017. https://doi.org/10.1145/3152465.3152467.
30. Lindhout P, Reniers G. What about nudges in the process industry? exploring a new safety management tool. J Loss Prev Process Indu. 2017;50:243–56. https://doi.org/10.1016/j.jlp.2017.10.006.
31. Loftus E, Loftus G, Messo J. Some facts about "weapon focus''. Law Hum Behav. 1987;11:55. https://doi.org/10.1007/BF01044839.
32. Lovreglio R, Fonzone A, dell'Olio L, Ibeas A. The role of herding behaviour in exit choice during evacuation. Procedia Soc Behav Sci. 2014;160:390–9.
33. Ma Y, Lee EWM, Shi M. Dual effects of guide-based guidance on pedestrian evacuation. Phys Lett A. 2017;381(22):1837–44. https://doi.org/10.1016/j.physleta.2017.03.050.
34. Mackworth NH. Visual noise causes tunnel vision. Psychon Sci. 1965;3:67–68.
35. Mas E, Suppasri A, Imamura F, Koshimura S. Agent-based simulation of the 2011 Great East Japan earthquake/tsunami evacuation: an integrated model of tsunami inundation and evacuation. J

Nat Disaster Sci. 2012;34(1):41–57. https://doi.org/10.2328/jnds.34.41.
36. Miura T. Coping with situational demands: a study of eye movements and peripheral vision performance. In: Gale AG, Freeman MH, Haslegrave CM, Smith P, Taylor SP, editors. Vision in vehicles. Amsterdam: North Holland Press; 1986. p. 205–16.
37. Moussaïd M, Helbing D, Theraulaz G. How simple rules determine pedestrian behavior and crowd disasters. Proc Natl Acad Sci. 2011;108(17):6884–8. https://doi.org/10.1073/pnas.1016507108.
38. Nilsson D, Frantzich H, Saunders W. Influencing exit choice in the event of a fire evacuation. Fire Saf Sci. 2009;9:341–52. https://doi.org/10.3801/IAFSS.FSS.9-341.
39. Nilsson D, Johansson A. Social influence during the initial phase of a fire evacuation-analysis of evacuation experiments in a cinema theatre. Fire Saf J. 2009;44(1):71–9. https://doi.org/10.1016/j.firesaf.2008.03.008.
40. Plainis S, Murray I, Chauhan K. Raised visual detection thresholds depend on the level of complexity of cognitive foveal loading. Perception. 2001;30:1203–12. https://doi.org/10.1068/p3117.
41. Raafat RM, Chater N, Frith C. Herding in humans. Trends Cognit Sci. 2009;13(10):420–8.
42. Recarte M, Nunes L. Mental workload while driving: effects on visual search, discrimination, and decision making. J Exp Psychol Appl. 2003;9:119–37. https://doi.org/10.1037/1076-898X.9.2.119.
43. Saint-Lot J, Imbert JP, Dehais F. Red alert: a cognitive countermeasure to mitigate attentional tunneling. New York: Association for Computing Machinery; 2020. p. 1–6.
44. Saloma C, Perez GJ, Tapang G, Lim M, Palmes-Saloma C. Self-organized queuing and scale-free behavior in real escape panic. PNAS. 2003;100(21):11947–52.
45. Schmidt S, Galea E, editors. Behaviour-Security-Culture (BeSeCu): human behaviour in emergencies and disasters: a cross-cultural investigation. Lengeric: Pabst Science Publishers; 2013.
46. Sieben A, Schumann J, Seyfried A. Collective phenomena in crowds–where pedestrian dynamics need social psychology. PLoS One. 2017;12(6): e0177328. https://doi.org/10.1371/journal.pone.0177328.
47. Tsurushima A. Modeling herd behavior caused by evacuation decision making using response threshold. In:. Davidsson P, Verhagen H, editors. Multi-agent-based simulation XIX. MABS2018. LNAI 11463. Springer; 2019. p. 138–52.
48. Tsurushima A. Reproducing symmetry breaking in exit choice under emergency evacuation situation using response threshold model. In: Proceedings of the 11th international conference on agents and artificial intelligence—volume 1: ICAART. INSTICC, SciTePress; 2019. p. 31–41. https://doi.org/10.5220/0007256000310041.
49. Tsurushima, A.: Symmetry breaking in evacuation exit choice: impacts of cognitive bias and physical factor on evacuation decision. In: van den Herik J, Rocha AP, Steels L, editor. Agents and artificial intelligence 11th international conference. ICAART2019. LNAI 11978. Springer; 2019. p. 293–316. https://doi.org/10.1007/978-3-030-37494-5_15.
50. Tsurushima A. Validation of evacuation decision model: an attempt to reproduce human evacuation behaviors during the Great East Japan earthquake. In: In Proceedings of the 12th international conference on agents and artificial intelligence (ICAART 2020)—volume 1; 2020; p. 17–27.
51. Tsurushima A. Herd behavior is sufficient to reproduce human evacuation decisions during the Great East Japan earthquake. In: Rocha A, Steels L, Van den Herik J, editors. Agents and artificial intelligence. ICAART 2020. Lecture notes in computer science, vol. 12613. Berlin: Springer; 2021. p. 3–25. https://doi.org/10.1007/978-3-030-71158-0_1.
52. Tsurushima A. Reproducing evacuation behaviors of evacuees during the Great East Japan earthquake using the evacuation decision model with realistic settings. In: Proceedings of the 13th international conference on agents and artificial intelligence—volume 1: ICAART. INSTICC, SciTePress; 2021. p. 17–27. https://doi.org/10.5220/0010167700170027.
53. Tsurushima A. Scochastic multi-objective decision analysis for crowd evacuation guidance using a single visual signage. In: 2021 IEEE international conference on systems, man, and cybernetics (SMC); 2021. p. 360–7.
54. Tsurushima A. Simulation analysis of tunnel vision effect in crowd evacuation. In: Rutkowski L, Scherer R, Korytkowski M, Pedryca W, Tadeusiewicz R, Zurada JM, editors. Artificial intelligence and soft computing. ICAISC 2021. Lecture notes in computer science, vol. 12854. Berlin: Springer; 2021. p. 506–18. https://doi.org/10.1007/978-3-030-87986-0_45.
55. Tsurushima A. Multi-objective risk analysis for crowd evacuation guidance using multiple visual signs. In: Proceedings of the 14th international conference on agents and artificial intelligence—volume 1: ICAART. INSTICC, SciTePress; 2022. p. 71–82. https://doi.org/10.5220/0010886400003116.
56. Wilensky U. NetLogo. Center for connected learning and computer-based modeling. Evanston: Northwestern University; 1999.
57. Williams LJ. Tunnel vision or general interference? Cognitive load and attentional bias are both important. Am J Psychol. 1988;101(2):171–91.
58. Xu Y, Huang HJ. Simulation of exit choosing in pedestrian evacuation with consideration of the direction visual field. Phys A Stat Mech Appl. 2012;391(4):991–1000. https://doi.org/10.1016/j.physa.2011.10.022.
59. Yang X, Wu Z, Li Y. Difference between real-life escape panic and mimic exercises in simulated situation with implications to the statistical physics models of emergency evacuation: the 2008 Wenchuan earthquake. Phys A Stat Mech Appl. 2011;390(12):2375–80. https://doi.org/10.1016/j.physa.2010.10.019.
60. Yuan Z, Jia H, Zhang L, Bian L. A social force evacuation model considering the effect of emergency signs. Simul Trans Soc Model Simul Int. 2017. https://doi.org/10.1177/0037549717741350.
61. Yue H, Guan H, Shao C, Liu Y. Simulation of pedestrian evacuation with affected visual field and absence of evacuation signs. In: 2010 sixth international conference on natural computation, vol. 8; 2010. p. 4286–90.
62. Zhou M, Dong H, Liu J, Yao X, Li Y. Modeling of crowd dynamics with emergency signs via modified social force model. In: 2018 IEEE 14th international conference on control and automation (ICCA); 2018. p. 235–40. https://doi.org/10.1109/ICCA.2018.8444225.